Inelastic processes versus diffraction effects: Polar-angle energy-loss spectra of the graphite K edge

R. Gunnella, I. Davoli, R. Bernardini, and M. De Crescenzi
Dipartimento di Matematica e Fisica, Sezione dell' Istituto Nazionale di Fisica della Materia, Università di Camerino, 62032 Camerino, Italy
(Received 14 March 1995)

We report the angular behavior of the reflection energy-loss features above the carbon K edge in highly oriented pyrolitic graphite. The intensity variations of the π^* and σ^* structures have been used to evaluate the fine details of the basic mechanism governing the interaction between primary electrons of low kinetic energy ($\sim$500 eV) and a core electron transition. We have considered the most probable scattering events, namely: single inelastic scattering, energy loss preceded by diffraction, and diffraction preceded by energy loss. In our experimental condition we have evidenced that the main channel of interaction is essentially constituted by inelastic scattering followed by diffraction processes. Our experiment resolves the degeneracy proposed by theoretical calculations that assign an equal probability to the two transitions assisted by elastic scattering. The energy-loss process does occur at a very small scattering angle from the primary beam direction (parallel-q exchanged) and this explains the capability for low-energy electrons to investigate the orientational dependence of the density of states and the bond-length direction of an adsorbed surface atom as currently done in surface x-ray-absorption measurements.

I. INTRODUCTION

The development of electron spectroscopies based on inelastic scattering fine structure is driven mainly by the need for structural methods which allow the investigation of the geometrical environment of different atomic species in the surface region. The EELFS (extended energy-loss fine structure) technique,[1] using low-kinetic-energy electrons (500–2000 eV) in the reflection geometry, has proven to be a useful tool for local structural investigation of clean surfaces, thin films, and chemisorbed species.[2,3] The main appeal of this technique, besides its very easy experimental accessibility, is the way in which the data are processed. The radial distribution function, coordination numbers, and thermal effects may be determined following the procedure used for EXAFS (extended x-ray-absorption fine structure) spectroscopy.[4]

In the last decade a considerable number of experimental and theoretical works has been devoted to assessing the equivalence of the structural determination obtained in experiments having an electron-gun source with those obtained using highly polarized synchrotron radiation.[5–7] The crucial point which guarantees this equivalence is to suppose valid the dipole approximation appearing in the matrix element of the electronic scattering. While in transmission-mode-detected EELFS (Ref. 8) the first Born approximation is widely accepted, the energy loss in the reflection mode deserves several criticisms connected with the large value of the transferred moment $\mathbf{q}$ which invalidates the dipole approximation.[9,10] In particular, Saldin has clearly shown that the dominant processes contributing to the EELFS spectrum are those involving elastic backscattering and small-angle energy-loss scattering.[11] This offered a suggestive explanation for the dominance of the dipole selection rule even in those cases where the experimental geometry should favor a large momentum being transferred. On the basis of this interpretation, the EELFS signal at the same time involves inelastic scattering of the incident beam and backscattering elastic events supplied by a reciprocal-lattice vector $\mathbf{G}$. These considerations, which are of fundamental importance every time a primary electron beam interacts with a solid surface, in our opinion need to be deeply investigated. Indeed a complete understanding of the energy-loss mechanism requires us to assess the contribution of the various mentioned processes. To this aim we performed angular-resolved near-edge spectra on HOPG (highly oriented pyrolitic graphite), and the observed intensity variations of the π^* and σ^* structures have been compared with the theoretical EELFS intensity. The main conclusion of this work is that for primary electrons of low kinetic energy ($E_p \geq 2\Delta E$), where ΔE is the energy loss, and the experimental geometry adopted in this work [the cylindrical mirror analyzer (CMA) electron analyzer], the dominant channel of interaction with a core electron is essentially constituted by inelastic scattering followed by diffraction processes ($L+D$). For a higher primary beam energy the other possible interaction, constituted by elastic scattering followed by energy loss, becomes more and more important, and the intensity ratio between the two processes approaches 1. Because of the tunability of this interaction mode obtained by varying the primary electron energy and the scattering geometry, a wider possibility in the investigation of both the bond-length direction and the electronic state symmetry of atoms on surfaces is provided by reflection energy-loss measurements at atomic core levels. At the moment this peculiarity is reserved

only to SEXAFS (surface-EXAFS) (Ref. 12) and XPD (x-ray photoelectron diffraction) measurements.[13]

After a brief description of the experimental apparatus in Sec. II, the formalism used in the calculation of the EELFS cross section is reported in Sec. III, where emphasis is placed on the existing parallel between EELFS and x-ray-absorption spectroscopy (XAS). Experimental results and theoretical considerations about the role of the possible diffraction processes during EELFS are discussed in Sec. IV. The conclusions of the work are reported in Sec. V.

II. EXPERIMENT

The experiment was carried out in a standard UHV system equipped with a single-pass CMA (cylindrical mirror analyzer) properly modified to detect the angular distribution of the outgoing electrons.[14] The modification consisted in screening 354° of the 360° circular ring of the usual CMA detection area. In this way a detection cone of 6° positioned at 42.6° with respect to the incident electron-beam direction was obtained.

The sample used was a HOPG freshly peeled off by an adhesive tape directly in the UHV system (better than 2×10^{-10} Torr). The low-energy electron-diffraction (LEED) pattern showed an array of spots with circular symmetry, testifying to the misoriented nature of the micro-single-crystalline structure around the c axis of the sample. This means that the sample has a random orientation within the ab planes, while it is well oriented along the c axis.

A primary beam energy of 500 eV and a modulation voltage of 0.5 V_{p-p} has been used to detect the electron energy distribution in first derivative mode. The parameters were chosen in order to achieve the best energy resolution during the energy-loss experiment (0.7–0.8 eV).

III. THEORY

As is well known in energy-loss spectroscopy, the Born approximation is applicable when the electron primary beam energy is at least seven times the ionization energy of the electronic level involved in the transition.[15] This condition is very rarely verified during an energy-loss experiment done in the reflection mode, and a different approach based on the distorted-wave Born approximation (DWBA) must be considered.[16] Following the work of De Crescenzi *et al.*,[5] the EELFS cross section in the DWBA can be written for the case of a collection of muffin-tin potentials as

$$\frac{d\sigma}{d\Omega}=4\frac{k_s}{k_i}\frac{k}{\pi}\sum_{L,L',n}\frac{|A(\mathbf{q}_n,\mathbf{G}_n)|^2}{q_n^4}\times\mathrm{Im}\{i^{l-l'}M_l(q_n)Y_L(\hat{q}_n)\times\tau^{0,0}_{L,L'}M_{l'}(q_n)Y_{L'}(\hat{q}_n)\}\ , \tag{1}$$

where the momentum transferred $\mathbf{q}_n=\mathbf{k}_i-\mathbf{k}_s+\mathbf{G}_n$ is the result of an energy loss $\Delta E=k^2$ of an incident electron with momentum $\mathbf{k}_i$, as scattered electron with momentum $\mathbf{k}_s$, and the interaction with the crystal by means of reciprocal-lattice vectors $\mathbf{G}_n$. In the present discussion we make the assumption that at electron energies characteristic of this spectroscopy ($E\geq500$ eV) substantial penetration of the electrons (10–15 Å) allows us to consider an interaction of electrons with a three-dimensional (3D) reciprocal lattice. This approximation could be questionable in an application to surfaces where only the two-dimensional reciprocal lattice is involved, because of the semi-infinite nature of the solid.[17] But in our case, or more generally far enough from the high end of the LEED region (500–600 eV), we may estimate a much greater number of probed planes in the solid making this spectroscopy experience genuine 3D structural effects. To properly deal with this problem a much more refined theory, taking into account full LEED wave functions, as proposed by Saldin,[11] is necessary but out of the aim of the present work. In Eq. (1) the EELFS cross section is written in atomic units of Ry, and is represented by the sum over all the momenta ranging from $q_{\min}=k_i-k_s$, and $q_{\max}=k_i+k_s$. Nevertheless it has been demonstrated by several authors[5,7,18] that the effective value of the momentum transfer cannot exceed the value of $\bar{q}_{\max}=\sqrt{\Delta E}$ during a reflection experiment.

Also, in Eq. (1) we have the 1 component of the matrix element of the transition operator $e^{i\mathbf{q}_n\mathbf{r}}$:

$$M_l(q_n)=\int_0^{r_s}\phi^0_{l_0}(r)j_l(q_nr)R_l(r)r^2dr\ , \tag{2}$$

written in terms of the spherical Bessel functions $j_l(q_nr)$. The terms $\phi^0_{l_0}(r)$ and $R_l(r)$ are the one-electron radial wave functions of the secondary electron in the initial and final states, respectively. The matrix element is calculated over the volume of the ionized atom of muffin-tin radius r_s.

With

$$\tau^{0,0}_{L,L'}=[(T^{-1}+G)^{-1}]^{0,0}_{L,L'} \tag{3}$$

we indicate the multiple-scattering operator obtained by inversion of the matrix built by means of the atomic scattering matrix T and the propagator G between different atomic sites in the solid.[5] $Y_L(\hat{q}_n)$'s are the real spherical harmonics of angular momentum (l,m), being the basis functions for the final-state multiple-scattering wave function. As can be seen from Eq. (1), only scattering processes in which the electron emitted by the ionized atom is backscattered by the surrounding atoms, give rise to a fine structure (EELFS) in the energy-loss spectrum.

Finally $A_n(\mathbf{q}_n,\mathbf{G}_n)$, which represents the weight of the diffraction accompanying the energy loss (direct and exchange process), is

$$A_n(\mathbf{q}_n,\mathbf{G}_n)=\sqrt{4\pi}\left[1\pm\frac{q_n^2}{|k_i-k|^2}\right]\rho(\mathbf{G}_n,\mathbf{k}_i,\mathbf{k}_s)\ , \tag{4}$$

which is related to the two-electron wave function through a Fourier transform

$$\Psi_i^+(\mathbf{R},\mathbf{k}_i)\Psi_s(\mathbf{R},\mathbf{k}_s)=\sum_{G_n}e^{i\mathbf{q}\cdot\mathbf{r}+i\mathbf{G}_n\cdot\mathbf{r}}\rho(\mathbf{G}_n,\mathbf{k}_i,\mathbf{k}_s)\ , \tag{5}$$

where $\mathbf{q}=\mathbf{k}_i-\mathbf{k}_s$.

It has been demonstrated that because of the $1/q_n^4$

dependence only the minimum momentum contributes to Eq. (1).[5,11] It is then possible, in a first approximation, to drop the index n in Eq. (1) and consider $q_n = q_{\min}$ hereafter in the paper. In this approximation, the calculation of Eq. (1) is done using two clusters of 66 and 70 carbon atoms (corresponding to a radius of about 6 Å) for the two symmetry-distinct ionization sites of the graphite structure. The cluster potential has been built following a well-established procedure used in XAS calculation.[19] The potential used was $X\alpha$. The maximum angular momentum used in the calculation was $l=4$.

In this work we have used the method of the extended continuum described by Tyson *et al.*[19] In this method, bound and continuum states are considered to have the same analytical behavior in terms of the same kind of Bessel and Hankel functions, as propagating waves to describe the final state of the secondary electron. In fact this method does not make any use of an outer sphere surrounding the whole cluster in order to properly describe the wave-function localization occurring in the case of the bound state. In the extended continuum method the interstitial constant potential is extended everywhere in space; also, electronic states with an energy greater than the interstitial potential but smaller than zero (i.e., bound states) are considered as a propagating solution of the Schrödinger equation.

The advantage of this method is to consider bound states as very narrow scattering resonances ultimately leaking away from the cluster region in a continuum state, instead of decaying exponentially as true bound states do. In this way the same single continuum calculation gives the energy separation between bound-state features and features of the continuum of the spectrum. Actually the main drawback of this method is the error introduced by the propagating wave normalization applied to the final bound state. This results in an underestimate of the bound-state transition strength.

We applied this method to the case of the graphite. In the K-edge excitation region two main features appear in the XAS spectrum due to the strong two-dimensional nature of this solid:[20–22] one narrow transition to a p_z (z along the c axis) symmetry π^*-band state near 285 eV, and one transition to a broader p_{x-y} σ^*-band 8 eV above the former one. The empty π^* band, which has been shown to be very flat over a large portion of the Brillouin zone from the theoretical band-structure calculation,[23,24] has been located by comparison with experiments 2 eV above the Fermi level and about 3 eV below the continuum threshold.[21,22] Due to this characteristic of the band structure, the transition to the π^* band can be thought as a transition to a well-localized state, excitonic in nature,[25] of different character from the σ^* transition, which is assumed to be a shape resonance of the continuum of the states.

To study these two prominent features of the EELFS spectrum, we use the extended continuum method properly modified to be applied in EELFS. The problem of the normalization of the wave function has been solved by comparing a theoretical calculation with polarized XAS experiment reported by Rosenberg, Love, and Rehn at the carbon K edge of graphite as shown in Fig. 1.[21] The

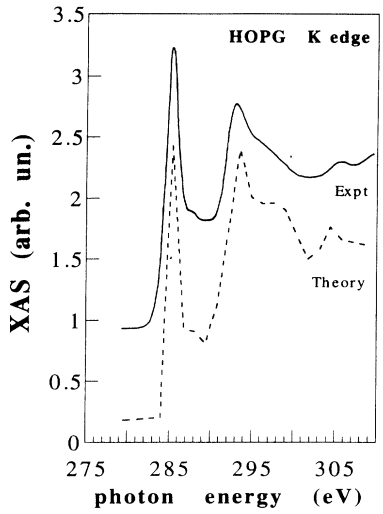

FIG. 1. Comparison between the x-ray-absorption measurements at the K-edge of graphite as reported by Rosenberg, Love, and Rehn (Ref. 21) (solid line), and full multiple-scattering calculation (dashed line). The data are collected near the "magic" angle (54°) used to average the polarization effects. The ionization threshold is located in the theoretical spectrum at 289 eV.

calculation has been convoluted with core-hole and instrumental broadening, and reproduces quite well all the main features present in the XAS spectrum. In particular the intensity of the two transitions (σ^* and π^*) under study can be well compared with the experimental ones. We conclude that in the case of graphite the extended continuum method is accurate enough to determine the transition amplitude, and it can also be used in the EELFS case to find the behavior of the two transitions as a function of the transferred momentum.

IV. RESULTS AND DISCUSSION

In Fig. 2, panel (a) shows a set of EELFS near-edge spectra detected above the carbon K edge of graphite. Several curves are collected as a function of the angle θ. The angle is measured from the normal to the surface (c axis), and the direction of the electron analyzer. In panel (b) the same curves are numerically integrated to better enhance the angular dependence of the σ^* and π^* structures.

The intensity of the two transitions π^* (285 eV) and σ^* (292 eV), as the peak-to-peak value of the first derivative spectrum, has been plotted in Fig. 3 for several values of the polar angle θ. This method gives the same results as those obtained by the nonderivative $N(E)$ spectra as demonstrated in quantitative Auger spectroscopy.[26] On the other hand, we preferred not to introduce additional artifacts due to the deconvolution of the numerically integrated spectra.

It appears clearly from Fig. 3 that the two features each have a different trend. While π^* has a bell shape

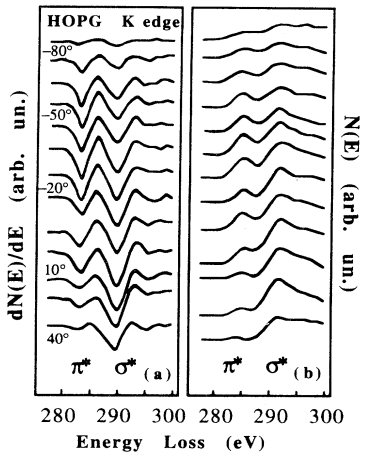

FIG. 2. (a) Energy-loss data at the K-edge HOPG detected as the first derivative of the electron yield $N(E)$, and as a function of the detection angle of the experimental apparatus discussed in the text. (b) Numerical integral of the energy-loss data shown in (a). π^* and σ^* features are indicated.

with the maximum located at about $-40°$ emission angle (corresponding to the c axis parallel to the incident electron beam) σ^* displays a monotonic behavior. The different anisotropies of the two structures are deeply connected with the layered nature of the graphite. Indeed, experimental data performed in the transmission mode have already shown the orientational dependence of the π^* and σ^* features.[20,27] The presence of a sizable orientation dependence also observed in the reflection mode is in our opinion the key to establishing the correct model of the energy-loss process.

In Fig. 4 we report schematically the wave-vector geometry involved in the energy-loss processes detected with our experimental apparatus. The advantage of the present experimental setup is that the transferred momentum can be considered constant in the modulus during the whole angular scan because of the fixed geometry between the incident beam and the analyzer aperture. Panel (a) reports the single inelastic scattering in which $\mathbf{k}_i$ and $\mathbf{k}_s$ are the wave vectors of the incoming and scattered primary electron beam, respectively, while $\mathbf{q}$ is the transferred momentum absorbed directly by the core electron transition. The limit of applicability of the dipole selection rule in the single inelastic model comes out from the huge amount of $\mathbf{q}$ required for the backscattering of the primary electrons. Alternatively, several authors[11,18,28–30] have proposed two competitive mechanisms in which the large part of the $\mathbf{q}$ is supplied by the sample lattice through an elastic reflection with a tridimensional reciprocal-lattice vector $\mathbf{G}$. The two mechanisms sketched in panels (b) and (c) can be described by the two pairs of equations

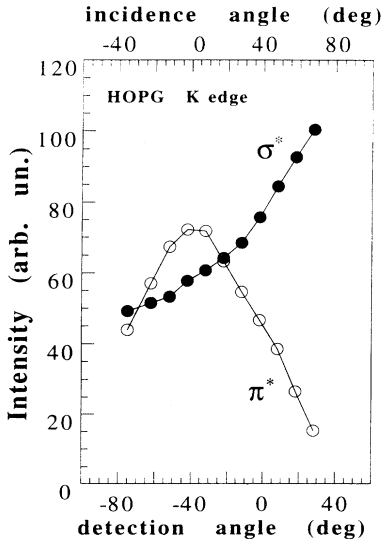

FIG. 3. Peak-to-peak intensity of the π^* and σ^* features of the HOPG K edge reported in Fig. 2(a). The angular behavior is reported both as a function of the angle between the c axis and the aperture of the electron analyzer, and between the c axis and the primary beam direction.

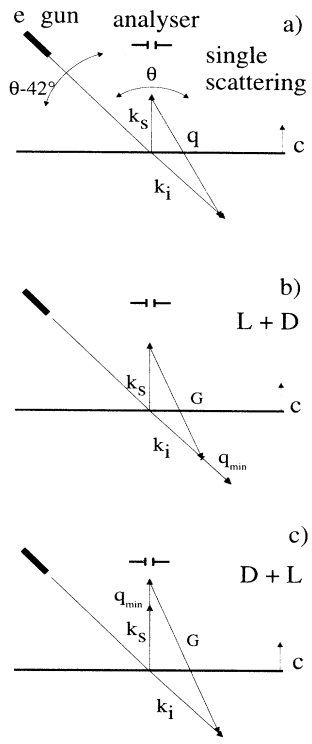

FIG. 4. Schematic pictures showing (a) single scattering event; (b) loss followed by a diffraction process; and (c) diffraction followed by a loss event. k_i and k_s are the incident and scattered electron momenta. $q_{\min}$ is the transferred minimum momentum, and G is the reciprocal-lattice wave vector. In (a) we also sketch the angular scan performed in this work by varying the angle θ (the angle between the collection direction and the direction normal to the surface).

$$\mathbf{k}_i' = \mathbf{k}_i - \mathbf{q}_{\min} , \quad \mathbf{k}_s = \mathbf{k}_i' - \mathbf{G} , \tag{6a}$$

$$\mathbf{k}_i = \mathbf{k}_s' + \mathbf{G} , \quad \mathbf{k}_s = \mathbf{k}_s' - \mathbf{q}_{\min} . \tag{6b}$$

Depending on the successive interaction between the primary electrons and the core transition and the crystalline lattice, two alternative processes have been identified: loss before diffraction ($L+D$) and diffraction before loss ($D+L$), respectively. Since the matrix elements of the two processes have the same probability of occurring, it is difficult to find an energy-loss experiment in which this degeneracy is clearly solved.[29–31] In previous experiments made both in the valence-band region (0–30 eV)[29] and the core near-edge region, the predominance of one of them has not been definitely resolved.[18,31] On the other hand, the strong difference concerning the actual amount of the wave vector $\mathbf{q}$ between the first model and the two other models is fundamental in assessing the validity of the dipole approximation. The $\mathbf{q}$ values involved in our experimental condition are 17 Å^{-1} for model (a) and 4 Å^{-1} for models (b) and (c). The main goal of the present work is to exploit the projection of the $\mathbf{q}$ vector with respect to the graphite c axis in order to discriminate between the ($D+L$) and the ($L+D$) mechanisms as a function of detection polar angle θ. In the experimental conditions provided by our apparatus during the angular scan, the momentum vector, according to the three models outlined above, assumes the following values:

$$\mathbf{q} = \mathbf{k}_i - \mathbf{k}_s , \tag{7a}$$

$$\mathbf{q} = q_{\min}[-\sin(\theta - 42°)\hat{x} - \cos(\theta - 42°)\hat{z}] , \tag{7b}$$

$$\mathbf{q} = q_{\min}(\sin\theta\hat{x} + \cos\theta\hat{z}) , \tag{7c}$$

where (7a), (7b), and (7c) specify the three models shown in Fig. 4, and θ is the detection angle, i.e, the angle between the direction of collection of the electrons and the normal to the surface, scanned during the experiment in the xz plane.

Calculation of the EELFS cross section proceeded in the following way. After the two transitions of interest were located on the energy scale, we calculated monopole, dipole, and successive terms in the expansion of the Eq. (1). In Fig. 5 are shown the different contributions in the case of the (b) event of Fig. 4, namely monopolar and dipolar contributions to the cross section. An averaging operation over the orientation of the ab plane of the graphite has been operated. In particular we reported a curve representing the peak anisotropy of the π^* transition which is due almost completely to the transition to a p_z symmetry state. The remaining curves are instead relative to the σ^* transition to a s, p_{x-y}, and p_z symmetry states.

We have found that transitions to states with $l=2$ or greater make a contribution of less than 3% to the whole cross section according to the result reported in Ref. 5. The π^* transition can be considered purely dipolar with a p_z symmetry, while the σ^* shape resonance contains, in addition to the p_{x-y} symmetry, a strong contribution from the monopolar transition (σ_s^*) and only a slight intensity from the p_z symmetry. This can explain the

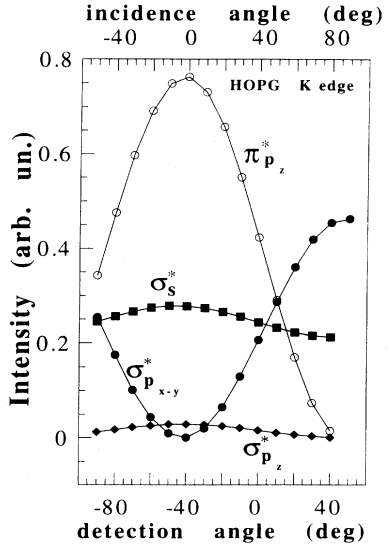

FIG. 5. Angular behavior of the various components of the HOPG near-edge features π^* and σ^* in the case of the ($L+D$) process. The π^* (open dots) is completely dipolar in character with p_z symmetry, while the σ^* transition (black symbols) accounts for several components with different symmetries: monopolar contribution (σ_s^*) and dipolar contribution ($\sigma^*_{p_{x-y}}$ and $\sigma_{p_z^*}$).

different behavior found in XAS (Ref. 21) when compared to the present EELFS results. While in XAS the absence of the monopolar contribution due to the selection rules can determine, in some polarization conditions, a great attenuation of the σ^* resonance with respect to the π^*, in EELFS the σ^* transition is definitely different from zero even for a minimum value of the momentum transferred.

Figure 6 reports, on the same scale, the evaluation of the intensity times q^4 for the prominent features of the K-edge graphite EELFS spectra and the three models outlined above. In the upper panel the single-scattering process gives rise to a low intensity (when the momentum value is taken into account), weakly varying with the angle of incidence of the primary electron beam. On the basis of these considerations and after a comparison with the experimental data reported in Fig. 3, the single-scattering interaction is ruled out as being responsible for the loss process. In the middle and lower panels of Fig. 6 the ($L+D$) and the ($D+L$) contributions are reported, respectively. We note that the two curves both for the σ^* (as a sum of the three main contributions of Fig. 5) and π^* transitions have the same trend in the two diffraction mechanisms, but are shifted in angle by an amount of about 42° due to the experimental geometry involved.

In doing this comparison it must be stressed that for the three processes we have retained the same prefactor $A_n(\mathbf{q}_n, \mathbf{G}_n)$ of Eq. (4), which is quite cumbersome to

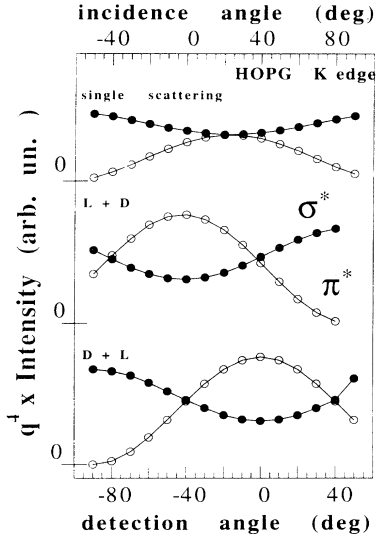

FIG. 6. Theoretical angular behavior of the EELFS intensity of the HOPG K edge of the π^* (open dots) and σ^* (black dots) features for the three loss mechanisms reported in Fig. 4. The σ^* intensity is due to the contribution of the three components as shown in Fig. 5.

determine. From the present analysis it is clearly shown that the $(D+L)$ process [Fig. 4(c)] makes a minor contribution compared to that of the $(L+D)$ process.

Moreover, it can be seen from Fig. 4 that the $(L+D)$ process needs a lower value of the crystal momentum necessary for the electron to reach the detector in comparison with the $(D+L)$ process, and for this reason it implies a larger $A_n(\mathbf{q}_n,\mathbf{G}_n)$ factor, which in the first approximation contains terms of the order of G^{-2}. From a direct comparison of the calculated anisotropy shown in Fig. 6 with experimental data reported in Fig. 3, it becomes clear that only the curve due to the matrix element of the $(L+D)$ process agrees over the whole emission angle range. The shift correctly reproduces the different projection of $q_{\min}$ with respect to the c axis as mathematically outlined by Eqs. (7b) and (7c), respectively. The simultaneous occurrence of the two events, although possible in principle, would give, as a result of the linear combination, a flatter curve with an intensity maximum shifted by 20° not supported by our experimental data.

Increasing the primary beam energy, with the corresponding lowering of the $q_{\min}$ value, a different trend in the relative intensities of the σ^* and π^* components of the K-edge spectrum has been found by Nassiopoulus and Cazaux[18] and Papagno *et al.*;[32] in their experiments they found a sizable increase of σ^* over π^* components for a normally incident beam. This behavior cannot be explained solely on the basis of a $(L+D)$ process, which on the other hand would show a predominance of π^* over σ^* for any primary beam energy. To explain this behavior one should keep in mind that for higher primary beam energies the $(D+L)$ mechanisms becomes more and more important. In fact, only in this case can one observe a predominance of σ^* over π^*, as reported from the bottom panel of Fig. 6.

By using first-order perturbation theory for the quantity reported in Eq. (5), we may give a rough estimate of the relative weights of the two $(L+D)$ and $(D+L)$ loss mechanisms. We write the quantity of Eq. (5) taking into account the incident and scattered wave functions for the first-order interaction with the solid periodic potential

$$\Psi_i^+(\mathbf{R},\mathbf{k}_i)\Psi_s(\mathbf{R},\mathbf{k}_s)=\frac{e^{i\mathbf{q}\cdot\mathbf{r}}}{V}\left[1+\sum_{G_n\neq 0}\frac{V_{\mathbf{G}_n}}{E_{\mathbf{k}_i}-E_{\mathbf{k}_i+\mathbf{G}_n}+i\mu}e^{i\mathbf{G}_n\cdot\mathbf{r}}+\frac{V_{\mathbf{G}_n}}{E_{\mathbf{k}_s}-E_{\mathbf{k}_s+\mathbf{G}_n}+i\mu}e^{-i\mathbf{G}_n\cdot\mathbf{r}}\right]. \tag{8}$$

From a direct comparison with Eq. (5), we find

$$A_n(\mathbf{q}_n,\mathbf{G}_n)\propto\rho(\mathbf{G}_n,\mathbf{k}_i,\mathbf{k}_s)=\left[\frac{V_{\mathbf{G}_n}}{E_{\mathbf{k}_i}-E_{\mathbf{k}_i+\mathbf{G}_n}+i\mu}+\frac{V_{-\mathbf{G}_n}}{E_{\mathbf{k}_s}-E_{\mathbf{k}_s-\mathbf{G}_n}+i\mu}\right] \tag{9}$$

Equation (8) in first approximation represents the three diffraction events accompanying the energy-loss process and sketched in Fig. 4. The two of particular interest, $(D+L)$ and $(L+D)$, which directly rely on the diffraction from the solid, are also reported in Eq. (9). A small complex part of the potential (μ) is introduced to dispose of divergences in Eqs. (8) and (9). In the two above equations the representation of the atomic core potentials by means of the Fourier transform components given by

$$\begin{aligned}V_{\mathbf{G}_n}&=\frac{1}{\Omega}\sum_{\mathbf{R}}\int_\Omega V(\mathbf{r}-\mathbf{R})e^{-i\mathbf{G}_n\cdot\mathbf{r}}d\mathbf{r}\\&=\frac{N}{\Omega}\int_\Omega-\frac{Ze^2}{r}e^{-i(r/\lambda)-i\mathbf{G}_n\cdot\mathbf{r}}d\mathbf{r}\\&=-\frac{8\pi}{\Omega_0}\frac{Z\lambda^2}{1+\lambda^2G_n^2}\end{aligned} \tag{10}$$

are considered valid for a Coulomb potential screened on the range of the Thomas-Fermi screening length λ, which in atomic units can be expressed in terms of the atomic number Z as $1/Z^{1/3}$. Ω_0 is the unit-cell volume.

The intensity ratio between the events $(D+L)$ and $(L+D)$ comes from the square modulus of the leading

terms of Eqs. (8) and (9) or what is the same:

$$\frac{I_{D+L}}{I_{L+D}} = \left| \frac{V_{G_{D+L}}}{V_{G_{L+D}}} \right|^2 = \left| \frac{1+\lambda^2 G_{L+D}^2}{1+\lambda^2 G_{D+L}^2} \right|^2 . \quad (11)$$

Considering an experimental geometry with a scattering angle of 180° (backscattering), it is very easy to estimate the quantity in Eq. (11) by substituting the value of the momentum provided by the solid $q_{\max}-q_{\min}$ and $q_{\max}+q_{\min}$ in the case of $(L+D)$ and $(D+L)$, respectively. In this way we obtain the following relation:

$$\frac{I_{D+L}}{I_{L+D}} = \left[\frac{1-\dfrac{2\lambda^2 q_{\min} q_{\max}}{1+\lambda^2 q_{\min}^2+\lambda^2 q_{\max}^2}}{1+\dfrac{2\lambda^2 q_{\min} q_{\max}}{1+\lambda^2 q_{\min}^2+\lambda^2 q_{\max}^2}} \right]^2 . \quad (12)$$

On the basis of Eq. (12), it can be observed that the contribution of the $(D+L)$ process increases at higher primary energy. In fact for $E_p=500$ eV the ratio I_{D+L}/I_{L+D} amounts to 30%, while for E_p it attains unity of the order of 2 keV.

Several years ago Cheung reported a similar orientational dependence of the carbon K edge, which resulted in good agreement with our data.[31] However, he considered only a single scattering picture with a value of $q=17$ Å^{-1} in demonstrating the complete predominance of the monopolar term on the observed features. Furthermore, using an integrated angular electron analyzer, he could not discriminate among the several directions of the momentum transferred in order to check the actual diffraction mechanisms.

More recently Hitchcock and Tyliszczak[33] studied the graphite K-edge angular dependence with an E_p of 2 keV, showing that the π^* contribution is also still present for an experimental geometry (glancing incidence for the primary beam and glancing detection) which should present an almost complete predominance of the σ^* component, according to the two main diffraction-mediated inelastic processes discussed in the present paper. Nevertheless it must be considered that in this particular geometry the q-exchanged value results to be of the same order of magnitude of $q_{\min}$ and parallel to the c axis. As a consequence the single-scattering [Fig. 4(a)] cannot be excluded on the basis of the argument of $1/q^4$, and a large-π^* component is observed in the spectrum. On the basis of all these energy-loss experiments, we stress that one can make use of particular experimental conditions to select the most suitable loss mechanism to investigate the character of the near-edge energy-loss structures.

V. CONCLUSIONS

We have shown that for anisotropic materials like HOPG it is possible to notice a stronger orientational dependence of the K-edge EELFS data if detected using an angular-resolved analyzer. The changes in the loss intensity collected for a primary beam of 500 eV as a function of the sample orientation indicate that $(L+D)$ with small-angle scattering is the most probable event, ruling out the single inelastic and $(D+L)$ mechanisms, the latter usually considered to be predominant in reflection mode experiments. This result is obtained by comparing calculations of the angular EELFS cross section in the framework of the DWBA and multiple-scattering evaluation of the final-state wave function. The importance of our investigation relies on the fact that at low primary beam energies the predominance of the $(L+D)$ process opens a wide field for applications. In fact, backscattered electrons can be used for studying the angular near-edge features' dependence on the atoms, molecules, and layers adsorbed on ordered surfaces. It may be possible to obtain selective structural and electronic information on the bond length. Indeed, the projection of the transferred q with respect to the normal to the surface can play the same role as the highly polarized electric field of the synchrotron radiation. For higher primary beam energy the weight of the $(D+L)$ process is found to increase considerably, becoming of the same order of magnitude as the $(L+D)$ one. In this way we explained the behavior of the near-edge features in highly anisotropic materials for the whole range of primary beam energies used.

ACKNOWLEDGMENT

The authors are indebted to C. R. Natoli, INFN (Istituto Nazionale di Fisica Nucleare) Frascati, for helpful discussions and suggestions.

[1] M. De Crescenzi, F. Antonangeli, C. Bellini, and R. Rosei, Phys. Rev. Lett. **50**, 1949 (1983).

[2] M. De Crescenzi and G. Chiarello, J. Phys. C **18**, 3595 (1985); M. De Crescenzi, CRC Crit. Rev. Solid State Mater. Sci. **15**, 279 (1989); Surf. Sci. **162**, 838 (1985); J. Vac. Sci. Technol. A **5**, 869 (1987); Surf. Sci. Rep. **21**, 89 (1995).

[3] T. Tyliszczak, F. Esposto, and A. P. Hitchcock, Phys. Rev. Lett. **62**, 2551 (1989).

[4] P. A. Lee, P. M. Citrin, P. Eisemberger, and B. M. Kincaid, Rev. Mod. Phys. **53**, 769 (1981); J. Stöhr, in *X-Ray Absorption, Principles, Applications, and Techniques of SEXAFS and XANES,* edited by D. C. Koningsberger and R. Prins (Wiley, New York, 1988), Vol. 92, p. 443.

[5] M. D. Crescenzi, L. Lozzi, P. Picozzi, S. Santucci, M. Benfatto, and C. R. Natoli, Phys. Rev. B **39**, 8409 (1989).

[6] P. Aebi, M. Erbudak, F. Vanini, D. D. Vvedensky, and G. Kostarz, Phys. Rev. B **41**, 11 760 (1990).

[7] D. K. Saldin and J. M. Yao, Phys. Rev. B **41**, 52 (1990); D. K. Saldin and Y. Ueda, *ibid.* **46**, 5100 (1992).

[8] B. M. Kincaid, A. E. Meixner, and P. M. Platzmann, Phys. Rev. Lett. **40**, 1269 (1978); W. L. Schaich, Phys. Rev. B **29**, 6513 (1984).

[9] F. Della Valle, G. Comelli, F. Zanini, R. Rosei, and G. Paolucci, Phys. Rev. B **38**, 19 335 (1988); G. Paolucci, A. Santoni, G. Comelli, K. C. Prince, and R. G. Agostino, *ibid.* **44**, 10 888 (1991).

[10]B. Luo and J. Urban, J. Electron Spectrosc. Relat. Phenom. **57**, 399 (1991).
[11]D. K. Saldin, Phys. Rev. Lett. **60**, 1197 (1988).
[12]P. H. Citrin, Surf. Sci. **299-300**, 199 (1994).
[13]S. A. Chambers, Surf. Sci. Rep. **16**, 261 (1992).
[14]I. Davoli, R. Bernardini, C. Battistoni, P. Castrucci, R. Gunnella, and M. De Crescenzi, Surf. Sci. **306**, 144 (1994).
[15]N. F. Mott and H. S. W. Massey, *The Theory of Atomic Collisions,* 3rd ed. (Oxford University Press, Oxford, 1965).
[16]H. A. Bethe and R. Jackiw, *Intermediate Quantum Mechanics,* 3rd ed. (Benjamin Cummings, Menlo Park, CA, 1986).
[17]M.-C. Desjonquères and D. Spanjaard, *Concept in Surface Physics,* Springer Series Surface Science Vol. 30 (Springer-Verlag, Berlin, 1993).
[18]A. G. Nassiopoulos and J. Cazaux, Surf. Sci. **149**, 313 (1985); **165**, 203 (1986).
[19]T. A. Tyson, K. O. Hodgson, C. R. Natoli, and M. Benfatto, Phys. Rev. B **46**, 5997 (1992).
[20]R. D. Leapman and J. Silcox, Phys. Rev. Lett. **42**, 1361 (1979).
[21]R. A. Rosenberg, P. J. Love, and V. Rehn, Phys. Rev. B **33**, 4034 (1986).
[22]D. Denley, P. Perfetti, R. S. Williams, D. A. Shirley, and J. Stöhr, Phys. Rev. B **21**, 2267 (1980).
[23]D. L. Greenaway, G. Harbeke, F. Bassani, and E. Tosatti, Phys. Rev. **178**, 1340 (1969).
[24]R. F. Willis, B. Fitton, and G. S. Painter, Phys. Rev. B **9**, 1926 (1974).
[25]E. J. Mele and J. J. Ritsko, Phys. Rev. Lett. **43**, 68 (1979).
[26]L. E. Davis, M. C. MacDonald, P. W. Palmberg, G. E. Riach, and R. E. Weber, *Handbook of Auger Electron Spectroscopy* (Perkin-Elmer, Eden Prairie, MN, 1977).
[27]M. M. Disko, O. L. Krivanek, and P. Rez, Phys. Rev. B **25**, 4252 (1982).
[28]R. L. Gerlach and A. R. Du Charme, Phys. Rev. A **6**, 1892 (1972); R. A. Bonham, J. Electron. Spectrosc. Relat. Phenom. **3**, 85 (1974).
[29]N. R. Avery, Surf. Sci. **111**, 358 (1981); F. P. Netzer and M. M. El Gomati, *ibid.* **124**, 26 (1983).
[30]G. Meister, P. Giesert, J. Holzl, and L. Fritsche, Surf. Sci. **143**, 547 (1984).
[31]T. T. P. Cheung, Phys. Rev. B **31**, 4792 (1985).
[32]L. Papagno, L. S. Caputi, M. De Crescenzi, and R. Rosei, Phys. Rev. B **26**, 2320 (1982).
[33]A. P. Hitchcock and T. Tyliszczak, Physica B **158**, 631 (1989).